Few-Body Systems manuscript No.
(will be inserted by the editor)

P. Niemann · H.-W. Hammer

Limit Cycles from the Similarity Renormalization Group

Received: date / Accepted: date

Abstract We investigate renormalization group limit cycles within the similarity renormalization group (SRG) and discuss their signatures in the evolved interaction. A quantitative method to detect limit cycles in the interaction and to extract their period is proposed. Several SRG generators are compared regarding their suitability for this purpose. As a test case, we consider the limit cycle of the inverse square potential.

Keywords similarity renormalization group · limit cycle

1 Introduction

Few-body systems with resonant interactions have universal properties independent of the details of the interaction at short distances [1]. If the scattering length a is much larger than the range of the interaction r_0, the Efimov effect can occur [2]: there is a geometric spectrum of three-body bound states with an accumulation of states at threshold. For identical bosons in the unitary limit, the Efimov spectrum satisfies the geometric scaling relation

$$\frac{E_3^{(n)}}{E_3^{(n+1)}} = \left(e^{\pi/s_0}\right)^2 , \tag{1}$$

where $s_0 = 1.00624\ldots$ is a transcendental number. In general, the value of s_0 depends on the symmetries of the three-body system, the number of interacting pairs, and the masses of the particles involved, but the form of the spectrum (1) is universal. The invariance of the spectrum under discrete scale transformations with the preferred scaling factor squared $e^{2\pi/s_0} \approx (22.7)^2$ can be understood as the consequence of a three-body interaction H governed by a renormalization group (RG) limit cycle [3; 4; 5]. The coupling constant $H(\Lambda)$ is then a periodic function of $\ln(\Lambda)$ with period π/s_0 where Λ is an ultraviolet cutoff in momentum space used to regulate the theory at short distances. More generally, the limit cycle will be manifest in observables through their log-periodic dependence on the scattering length or other control parameters of the system [1]. The period of this log-periodic behavior is again determined by the discrete scaling factor which is the key quantity determining the properties of the limit cycle.

The universal Efimov spectrum and related higher-body bound states have been observed in ultracold atomic gases in a variety of experiments with different atom species [6; 7; 8]. In heteronuclear mixtures the scaling factors can be significantly smaller than for ideal bosons. For example, in a mixture of ^{6}Li and ^{133}Cs atoms, the ratio of subsequent ^{133}Cs-^{133}Cs-^{6}Li bound states is predicted to be

Institut für Kernphysik, Technische Universität Darmstadt, 64289 Darmstadt, Germany
ExtreMe Matter Institute EMMI, GSI Helmholtzzentrum für Schwerionenforschung GmbH, 64291 Darmstadt, Germany

$(4.88)^2$. Such heteronuclear Efimov states have recently been observed in experiment and the prediction of the scaling factor was confirmed [9; 10]. Finally, we note that the Efimov effect also provides a universal binding mechanism for S-wave states in weakly-bound nuclei. However, an observation of the discrete scaling relation between different states in one nucleus has proven elusive to date since the known S-wave halo nuclei have no excited states. (See Ref. [11] for a review.)

Here, we investigate the manifestation of RG limit cycles in the similarity renormalization group (SRG). The SRG was developed independently by Wegner [12] and by Glazek and Wilson [13]. In recent years, it has become a standard tool to soften nuclear interactions for improved convergence in many-body calculations [14; 15]. The SRG generates a continuous series of unitary transformations of the Hamiltonian from the evolution with a flow parameter s. As the RG flow evolves, the interaction is typically softened at the expense of introducing induced many-body forces. Ideally, the evolution is carried out to a value s such that the interaction is softend enough to achieve convergence in many-body calculations without generating large contributions from induced many-body forces. Recent advances in SRG technology have, e.g., allowed to extend ab initio calculations to P-shell nuclei [16] or perturbative neutron matter calculations with consistent three-body forces [17]. The success of SRG methods in nuclear physics motivates our study of the manifestation of RG limit cycles within the SRG.

The emphasis of this work is on formulating criteria for detecting a limit cycle in the evolved interaction.[1] In particular, we study the numerical extraction of the discrete scaling factor. A long term goal of our work is the derivation of the limit cycle in the pionless EFT for the nuclear three-body system. While it is generally assumed that the pionless EFT in which the Efimov effect and corresponding limit cycle are manifest appears as the low-energy limit of a more fundamental chiral EFT with explicit pions, no explicit derivation has ever been given. Our work provides a first step towards this goal. As a test case, we investigate the attractive inverse square potential which is known to have an exact limit cycle beyond a critical coupling strength. For convenience, we will use natural units with $\hbar = m = 1$ in the following.

2 SRG Basics

We start with a brief review of the basic properties of the SRG. A more detailed discussion can be found in Refs. [15; 18].

The SRG generates a continuous series of unitary transformations on the Hamiltonian governed by a flow parameter s:

$$H(s) = U(s)H(s=0)U(s)^\dagger = T + V(s) \; , \tag{2}$$

where $U(s)$ is a unitary operator. Often the kinetic energy is left unchanged per definition, such that the SRG generates an evolution of the interaction potential V. Defining the anti-Hermitian operator $\eta(s) = (\frac{d}{ds}U(s))U(s)^\dagger = [G(s), H(s)]$, the evolution equation for the Hamiltonian can be written as

$$\frac{dH(s)}{ds} = [[G(s), H(s)], H(s)] \; , \tag{3}$$

where the Hermitian operator $G(s)$ is called the generator of the SRG transformation. The generator G is often taken independent of s. A frequent choice for G is the kinetic energy T. In this case, the differential equation can be written as

$$\frac{dV}{ds} = 2TVT - VTT - TTV + TVV + VVT - 2VTV \; . \tag{4}$$

If we consider a two-body system with identical particles, we can write the flow equation for the two-body interaction V_2 in the space of relative momenta as

$$\frac{d}{ds}\langle p|V_2|q\rangle = -(p^2-q^2)^2 \langle p|V_2|q\rangle + \int_0^\infty \frac{d^3k}{(2\pi)^3} (p^2+q^2-2k^2)\langle p|V_2|k\rangle\langle k|V_2|q\rangle \; . \tag{5}$$

[1] We note that a limit cycle will also be manifest in physical observables through universal scaling relations [1].

The evolution of partial waves decouple in the two-body system, thus Eq. (5) holds for every partial wave. In this representation one can recognize a major characteristic of the SRG with the T generator. Clearly, the SRG transformation has a fixed point if $H(s)$ commutes with T, i.e. $H(s)$ is diagonal.

For weak interactions, the second term in Eq. (5) can be neglected and the solution is simply

$$\langle p|V_2(s)|q\rangle = \langle p|V_2(0)|q\rangle \exp(-s(p^2-q^2)^2)\,. \tag{6}$$

All non-diagonal matrix elements approach zero during the evolution and thus a decoupling between low-energy and high-energy matrix elements is achieved. Although the second term in Eq. (5) typically can not be neglected, the suppression of non-diagonal matrix elements is a dominant part of the full SRG evolution using the T generator. The approximate expression (6) also suggests to interpret

$$\lambda \equiv s^{-1/4} \tag{7}$$

as an effective momentum cutoff. Thus the evolution starts at $s = 0$ corresponding to $\lambda = \infty$ and as s increases, the effective momentum cutoff λ is lowered.

In this work, we also use two alternative generators, which are functions of the kinetic energy. They were introduced by Li, Anderson, and Furnstahl with the aim to obtain a more efficient evolution which is crucial for identifying limit cycles [19]. We refer to them as exponential generator, G_e, and inverse generator, G_i:

$$\begin{aligned} G_e &= -\sigma^2 \exp(-T/\sigma^2)\,, \\ G_i &= \frac{-\sigma^2}{1+T/\sigma^2}\,, \end{aligned} \tag{8}$$

where σ is an arbitrary parameter with dimensions of momentum. Both generators have a power series expansion in T. For small momenta $q \ll \sigma$, they approach T up to a constant which cancels out in η. So depending on the parameter σ, there is a separation into a low-energy region, where the two generators behave like the T generator and a high-energy region, where the SRG evolution is suppressed. A detailed discussion of these generators can be found in Ref. [19].

Since σ has dimensions of momentum, the translation of s to an effective momentum cutoff is more subtle than for the T generator. The solutions of Eq. (5) in the weak interaction limit are

$$\langle p|V_2(s)|q\rangle = \langle p|V_2(0)|q\rangle \exp[-s\sigma^2(q^2-p^2)(e^{-p^2/\sigma^2}-e^{-q^2/\sigma^2})]\,, \quad \text{for } G_e\,, \tag{9}$$

and

$$\langle p|V_2(s)|q\rangle = \langle p|V_2(0)|q\rangle \exp\left[-s\sigma^2(q^2-p^2)\left(\frac{1}{1+p^2/\sigma^2}-\frac{1}{1+q^2/\sigma^2}\right)\right] \quad \text{for } G_i\,. \tag{10}$$

Thus the effective momentum cutoff is $\lambda \sim \sigma^{-1}s^{-1/2}$. The constant σ is irrelevant for the parametric dependence on s. Setting it to one, we define the effective momentum cutoff

$$\lambda_a \equiv s^{-1/2} \tag{11}$$

for the exponential and inverse generators from Eq. (8). This will have important consequences when extracting limit cycle periods from the evolved interaction below.

3 Renormalization of the $1/R^2$-Potential

In the following, we discuss the quantum mechanical $1/R^2$ potential as a test case. This is a singular potential which displays an exact limit cycle. We start by reviewing the renormalization of the $1/R^2$ potential in an effective field theory framework. Here, the limit cycle becomes manifest in the behavior of a counter term. We follow the discussion in Ref. [20] where further details can found. In the next section, we investigate the $1/R^2$ potential in the SRG framework and provide general criteria for isolating limit cycle behavior in the interaction.

The $1/R^2$ potential can be written as

$$V(R) = \frac{c}{R^2} \tag{12}$$

with $R := |\mathbf{R}|$ and c a coupling constant. For subcritical couplings $c > -\frac{1}{4}$, the potential is well behaved and leads to a unique solution of the Schrödinger equation. For critical and supercritical values $c \leq -\frac{1}{4}$, however, the potential is singular and displays a limit cycle. In this case, it is useful to define a parameter ν that characterizes the period of the limit cycle via $\nu := \sqrt{-c - \frac{1}{4}}$,

The momentum-space representation of the potential can be defined via a Fourier transform in D dimensions,

$$V(Q) = \lim_{D\to 3} \int d^D\mathbf{R}\, e^{i\mathbf{Q}\cdot\mathbf{R}}\, V(R) = \frac{2\pi^2 c}{Q}\,, \tag{13}$$

where Q is the momentum transfer [20].

In the following, we consider only S-waves. For the momentum space matrix elements of the S-wave projected potential, we get

$$V(p,q) = 2\pi^2 c \left(\frac{\theta(p-q)}{p} + \frac{\theta(q-p)}{q} \right)\,, \tag{14}$$

where q (p) are the incoming (outgoing) momenta. The physical observables can be obtained from the Lippmann-Schwinger equation

$$t_E(p,k) = V(p,k) + \frac{1}{2\pi^2} \int_0^\Lambda \frac{dq\, q^2}{E - q^2 + i\epsilon} V(p,q) t_E(q,k)\,, \tag{15}$$

where $E = k^2$ is the total energy and the scattering phase shifts are given by

$$k \cot\delta = ik - \frac{4\pi}{t_E(k,k)|_{E=k^2}}\,. \tag{16}$$

The bound states are given by the solutions of the corresponding homogeneous equation. As discussed in [20], Eq. (15) has no unique solution for $\Lambda \to \infty$ if $c < -\frac{1}{4}$ and requires renormalization. We regulate Eq. (15) with a sharp momentum cutoff Λ and absorb the cutoff dependence by introducing a momentum independent counterterm $\delta V(\Lambda)$.

$$V(p,q) \Rightarrow V(p,q) + \delta V(\Lambda) = 2\pi^2 c \left(\frac{\theta(p-q)}{p} + \frac{\theta(q-p)}{q} + \frac{H(\Lambda)}{\Lambda} \right)\,. \tag{17}$$

Demanding invariance of the zero-energy solution under changes of Λ, one finds

$$H(\Lambda) = \frac{1 - 2\nu \tan(\nu \ln(\Lambda/\Lambda_*))}{1 + 2\nu \tan(\nu \ln(\Lambda/\Lambda_*))} = 1 - 4\nu^2 \ln(\Lambda/\Lambda_*) + \dots\,, \tag{18}$$

where Λ_* is a low-energy constant. Including this counterterm in Eq. (15) keeps all low-energy observables fixed when Λ is varied. One can immediately see that the counterterm $H(\Lambda)$ displays a limit cycle with a preferred scaling factor $\exp(\pi/\nu)$ since tan is a periodic function with period π. If the cutoff Λ is changed by multiples of $\exp(\pi/\nu)$, the counterterm returns to the same value.

The bound state spectrum satisfies a geometrical scaling relation analog to the Efimov case,

$$\frac{E^{(n)}}{E^{(n+1)}} = e^{2\pi/\nu}\,, \tag{19}$$

and presents an ideal test case for the application of SRG methods to limit cycles. In the following section, we will investigate the limit cycle in the inverse square potential using the SRG framework.

4 $1/R^2$ Potential and SRG

In this section, we consider the $1/R^2$ potential in the SRG framework. Since the SRG is a unitary transformation, all observables stay constant during the evolution by definition. So in contrast to the explicit construction of the counterterm in the effective field theory treatment of the previous subsection, we need to extract a signal for the limit cycle from the evolved interaction. In order to define such a signal, we investigate the SRG evolution of the $1/R^2$ potential for critical and subcritical couplings and different generators.

Before we proceed, we specify our units. One free length scale l_0 is present in our framework. Therefore, all dimensionful quantities are given in units of l_0.

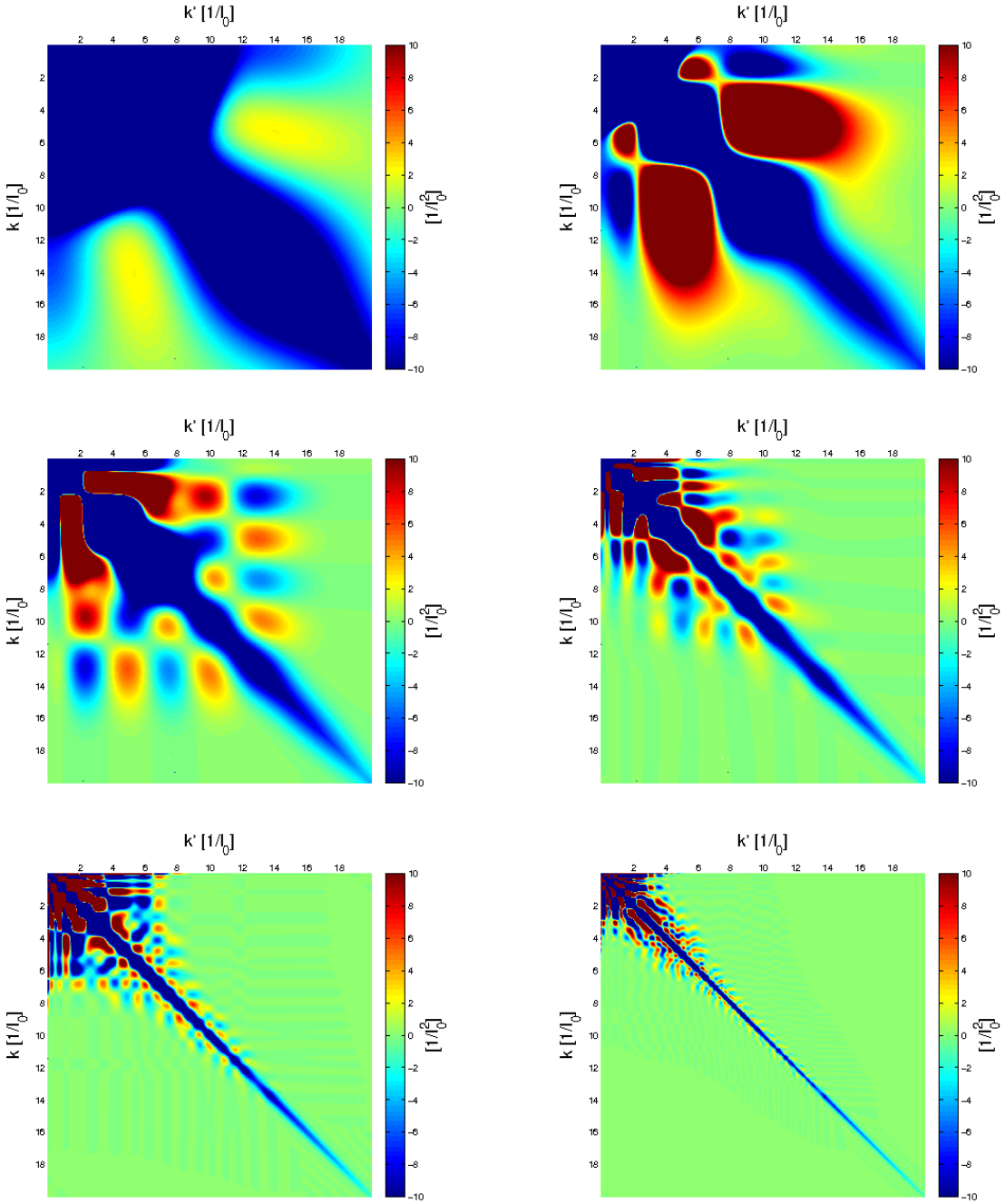

Fig. 1 Evolution of the S-wave $1/R^2$ potential for the T generator with $\nu = 9$ and initial cutoff $\Lambda = 20\ l_0^{-1}$. $V(k, k', \lambda)$ is shown for $\lambda \approx 21.09$, 13.67, 8.86, 5.74, 3.72 and 2.41 in units of $[1/l_0]$ from top left to bottom right.

4.1 Qualitative Features

First, we consider the standard T generator for the SRG transformation. In Fig. 1, we show the evolution of the potential for $\nu = 9$ and an initial cutoff in Eq. (15) of $\Lambda = 20\ l_0^{-1}$. Introducing this regulator is required in order to insure that Eq. (15) has a unique solution.

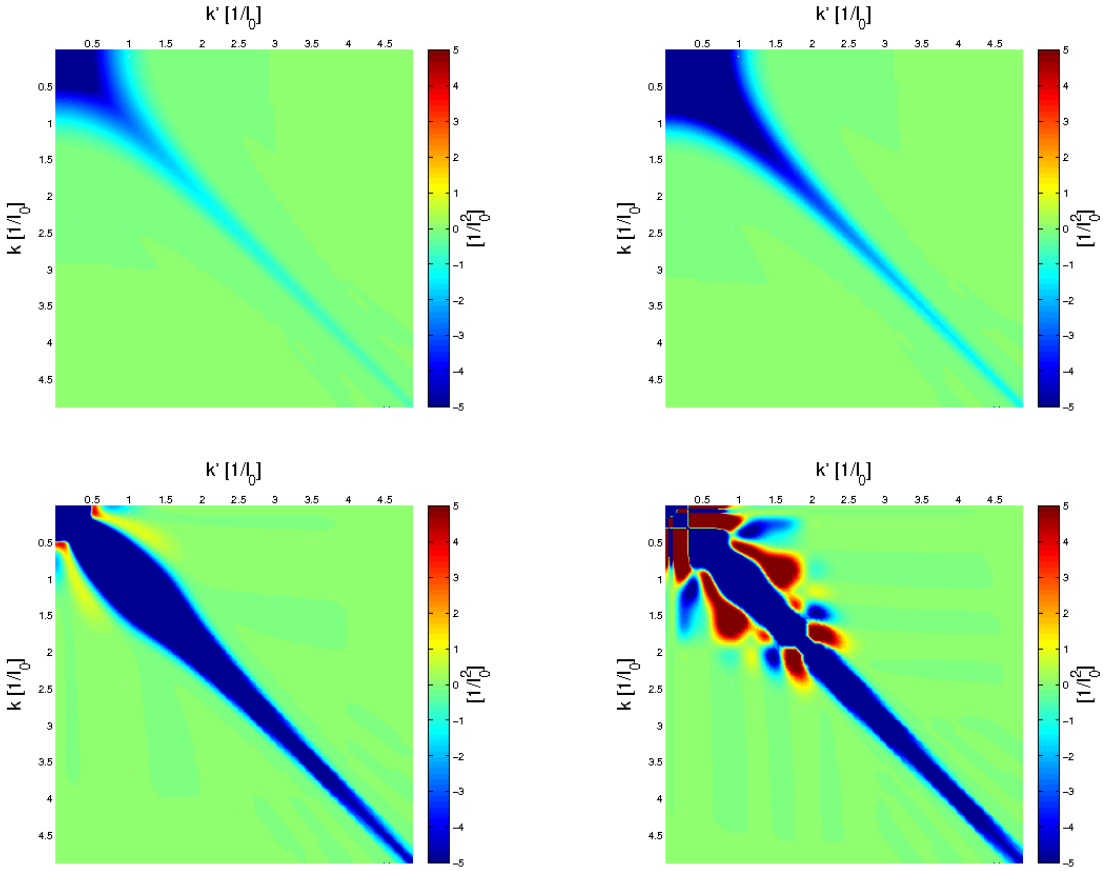

Fig. 2 S-wave $1/R^2$ potential evolved with the T generator to $\lambda = 1\ l_0^{-1}$ with initial $\Lambda = 20\ l_0^{-1}$. The potential strengths are $c = -0.125$, $c = -0.25$, $c = -0.25 - 1^2$ and $c = -0.25 - 2^2$ in the order from top left to bottom right.

Changing the value of Λ corresponds to changing the short-distance behavior of the starting interaction. We leave Λ fixed and investigate the dependence of the interaction on the SRG cutoff λ that is directly related to the flow parameter s. Striking is the appearance of separated regions in the potential with positive and negative sign. To make them clearly visible, we choose a rather small maximum value for the coloring of the potential. As the evolution progresses, these regions are constantly emerging and vanishing while the total number of regions increases. At the beginning of the evolution, two positive valued regions appear. During the further progress more and more positive and negative regions emerge. The size of these structures also decreases, which is related to the general suppression of off-diagonal matrix elements in the SRG evolution for the T generator. In the last picture, one can clearly see the large number of small regions. We also note that this behavior occurs on a logarithmic scale of the flow parameter s.

To confirm that the appearance of the oscillatory behavior is indeed related to the limit cycle, we have evolved $1/R^2$ potentials with subcritical coupling $c > -\frac{1}{4}$ where no limit cycle occurs and critical couplings $c \leq -\frac{1}{4}$ where it is present. In Fig. 2, four potentials are depicted, which were all evolved to $\lambda = 1\ l_0^{-1}$. All parameters of the potentials except for the coupling constant c are kept constant. For $c < -\frac{1}{4}$, the scaling factor is given by $\exp(\pi/\nu)$ with $\nu = \sqrt{-c - \frac{1}{4}}$. Thus, if c approaches the critical value $-\frac{1}{4}$ the scaling factor diverges. In Fig. 2, the evolved potentials beneath and at the critical value do not exhibit the oscillatory behavior. Only the effective diagonalization of V from the SRG transformation is clearly visible. For $\nu = 1$, two separated regions with opposite signs are observable up to this point in the evolution and for $\nu = 2$ several structures are already visible. This observation

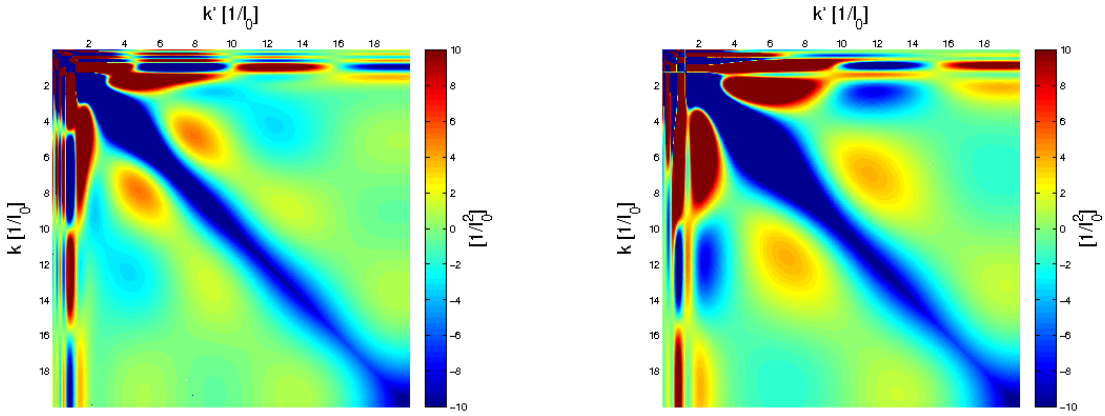

Fig. 3 Evolved $1/R^2$ potential with parameters $\nu = 9$, $\Lambda = 20\ l_0^{-1}$ and $\sigma = 2\ l_0^{-1}$ for G_e and G_i. Left panel: Evolution with the exponential generator G_e to $\lambda_a \approx 8.35\ l_0^{-1}$. Right panel: Evolution with the inverse generator G_i to $\lambda_a \approx 10.75\ l_0^{-1}$.

clearly supports our conjecture that the appearance of the oscillatory features is related to the limit cycle.

Next, we consider the inverse and exponential generators. We expect a similar qualitative signature of the limit cycle. However, the alternative generators contain a free dimensionful parameter σ which divides the potential into two different regions. For small momenta compared to σ, the exponential and inverse generators reduce to the T generator. For large momenta, the generators approach zero and the evolution is suppressed. As an example, we have plotted the evolved potential for $\nu = 9$, $\Lambda = 20\ l_0^{-1}$, $\sigma = 2\ l_0^{-1}$ in Fig. 3 for both the inverse and the exponential generator.

Notable is the fact that the oscillatory features become compressed in a rather small area in the $k - k'$ plane, whose size depends on σ. We remark that the qualitative behavior of the exponential and inverse generators are very similar. Thus, we will not distinguish their traits here. As for the standard T generator, the oscillatory structures only appear if the coupling constant is supercritical.

4.2 Discrete Scaling Factor

Next we focus on the question of how to extract the discrete scaling factor as the main characteristic of the limit cycle from the evolved potential. To observe a log-periodic signal, we investigated several different strategies, which we will discuss in the following.

First, we have investigated the possibility to isolate the oscillatory feature by projecting on the momentum independent part of the evolved potential. Assuming that the short-range part of the evolved potential can be expanded as

$$V(k, k', \lambda) = C_0(\lambda) + \frac{C_2(\lambda)}{2}(k^2 + k'^2) + \dots\ , \tag{20}$$

we have investigated the possibility to extract the preferred scaling factor from the λ dependence of C_0. In particular, we considered the quantities

$$I_1(\lambda) \equiv \int\int d^3k\, d^3k'\, V(k, k', \lambda) \qquad \text{and} \qquad I_2(\lambda) \equiv \int d^3k\, V(k, k, \lambda)\ . \tag{21}$$

$I_1(\lambda)$ is the projection of the evolved potential whereas $I_2(\lambda)$ is the projection of the diagonal part of the evolved potential. In both cases, we were not able to detect any clear signals of the limit cycle.

Second, we examined the diagonal elements of the evolved potential $V(p, p, s)$ in dependence of the flow parameter. This is motivated by the diagonalizing factor $\exp(-s(p^2 - q^2)^2)$ from Eq. (6). On the diagonal of the potential matrix incoming and outgoing momenta are identical, so that the exponential

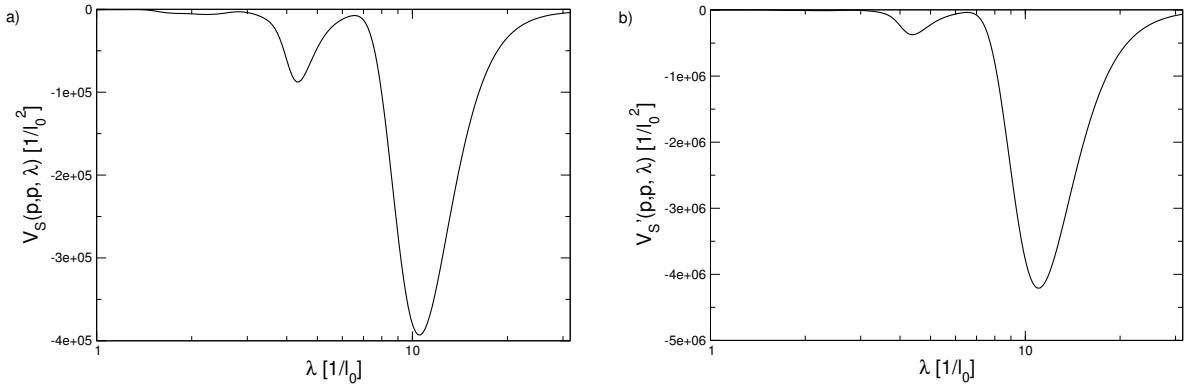

Fig. 4 (a) Diagonal element $V(p,p,\lambda)$ in dependence of λ for $p \approx 0.84\ l_0^{-1}$. (b) $V'(p,p,\lambda)$ from Eq. (22) in dependence of λ for $p \approx 0.84\ l_0^{-1}$. The parameters of the potential are $\nu = 9$ and $\Lambda = 20\ l_0^{-1}$. The evolution was carried out with the standard T generator.

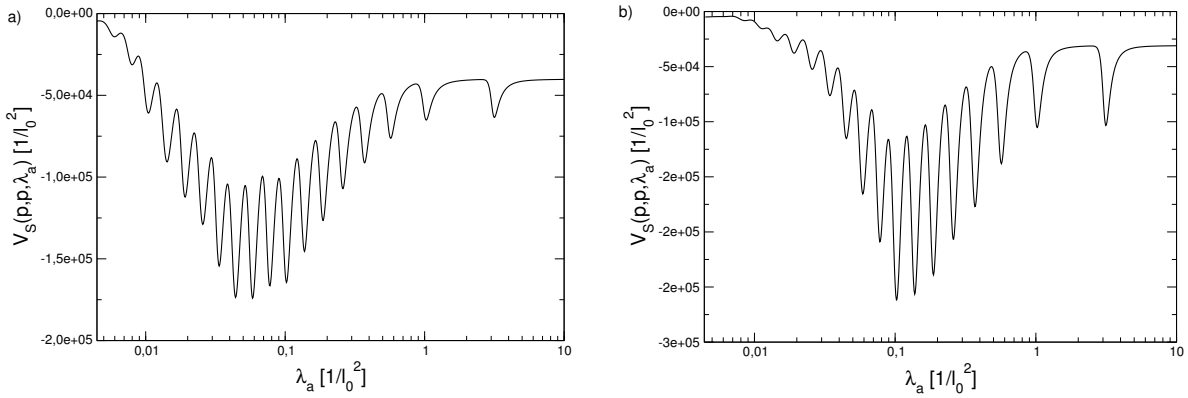

Fig. 5 Evolution of the diagonal elements $V(p,p,\lambda_a)$ with $\nu = 11$, $\Lambda = 30\ l_0^{-1}$ and $\sigma = 0.05\ l_0^{-1}$. (a) Applied exponential generator with $p \approx 1.19\sigma$ (b) Applied inverse generator evolved with $p \approx 1.55\sigma$.

function is one. Hence, the diagonal elements are the only ones, which do not approach zero during the evolution. So, we expect a log-periodic signal to be most prominent on the diagonal. A similar strategy was followed by Glazek [21] in the analysis of a discrete model displaying a limit cycle.

T generator. We start with the standard T generator. In Fig. 4(a) a typical diagonal element is depicted in dependence of the flow parameter. The diagonal elements show some irregular oscillations but a clear signature of the limit cycle period can not be extracted. This is also the case if we subtract the initial potential from the evolved potential and multiply by λ in order to isolate the SRG analog of the counterterm H from Eq. (17) above:

$$V'(p,p,\lambda) = (V(p,p,\lambda) - V(p,p,\lambda=\infty)) \cdot \lambda\,, \qquad \text{where} \qquad \lambda = s^{-1/4}\,. \tag{22}$$

In Fig. 4(b), we show $V'(p,p,\lambda)$ from Eq. (22) for the same diagonal matrix element as in Fig. 4(a). Again a clear signature of the limit cycle period could not be extracted. This was also the case if different powers of λ were used in Eq. (22).

Alternative generators. Using the standard T generator only very few irregular oscillations can be observed. Therefore, we try the same strategy with the exponential and inverse generators that allow for a further evolution in s. Here, a completely different behavior is found if momenta of order σ are considered. In Fig. 5, we plot a diagonal element with momentum p close to the parameter σ in dependence of the flow parameter for both generators. One can now clearly see regular oscillations for both generators. The graphs look like a log-periodic function multiplieded with another slowly-varying function.

An example with explicit values is given in Table 1. The extracted distances between the maxima and minima are constant to about 5%, except for the first few oscillations at large values of λ_a which is

oscillation	$\nu = 11$		$\nu = 5$	
	maxima	minima	maxima	minima
1	2.94	3.08	3.26	3.36
2	1.76	1.80	2.11	2.11
3	1.52	1.54	1.91	1.91
4	1.42	1.43	1.87	1.85
5	1.38	1.39	1.83	1.81
6	1.36	1.36	1.85	1.80
7	1.35	1.34	1.84	1.79
8	1.31	1.32		1.78
9	1.33	1.33		
10	1.34	1.33		
11	1.30	1.31		
12	1.33	1.31		
13	1.34	1.34		
14	1.38	1.35		
15	1.36	1.36		
16	1.33	1.31		
17		1.34		

Table 1 Examples of extracted ratios $\lambda_a^{(i)}/\lambda_a^{(i+1)}$ for the exponential generator, where the $\lambda_a^{(i)}$ are the flow parameter values of the maxima (minima) of $V(p, p, \lambda_a)$ with $p \approx 1.19\sigma$ for $\nu = 11$ and $\nu = 5$. The parameter values are $\Lambda = 30\, l_0^{-1}$ and $\sigma = 0.05\, l_0^{-1}$. The exact scaling factors are $\exp(\pi/11) \approx 1.33$ and $\exp(\pi/5) \approx 1.87$.

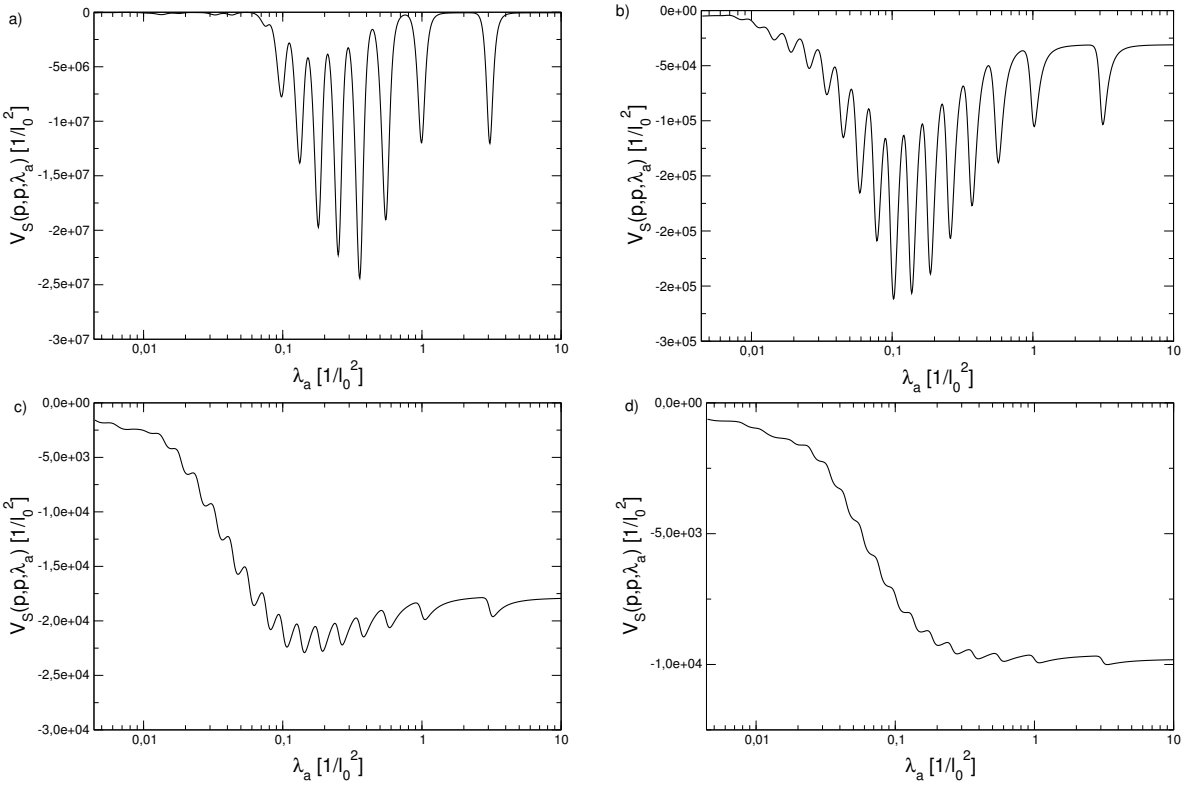

Fig. 6 Diagonal elements $V(p, p, \lambda_a)$ evolved with the inverse generator for four different momenta p with constants $\nu = 11$, $\Lambda = 30\, l_0^{-1}$ and $\sigma = 0.05\, l_0^{-1}$: (a) $p \approx 0.96\sigma$, (b) $p \approx 1.55\sigma$, (c) $p \approx 2.68\sigma$, (d) $p \approx 4.88\sigma$.

probably caused by finite cutoff effects. The period depends on the strength of the initial potential ν. Larger values of ν result in smaller periods. We find that the extracted periods are in good agreement with the exact formula $\exp(\pi/\nu)$. The agreement is better for larger values of ν, where more oscillations can be seen and the period can be determined more accurately.

We will now elaborate on the appearance of the oscillations on the diagonal. To this effect, the diagonal elements $V(p, p, \lambda_a)$ are displayed in Fig. 6 as a function of λ_a for four different momenta.

The clearest oscillations can be extracted in the region $p \approx \sigma$. For larger momenta, the amplitudes of the oscillations become smaller, cf. Fig. 6(c) and (d). If p is even further increased, the oscillations disappear. Figure 6 (a) demonstrates that choosing momenta smaller than σ leads to fewer oscillations on the diagonal. If p is even further decreased, the number of oscillations with large amplitude is reduced and the graph resembles the diagonals of potentials evolved with the T generator. This behavior is expected since the inverse and exponential generators reduce to the standard T generator for small momenta p. We briefly return to Fig. 6(b). For smaller λ_a, the amplitude of the oscillation decreases until no oscillation is visible anymore. The number of observable oscillations strongly depends on σ. Typically, they can be seen until λ roughly equals σ.

In summary, we find a clear signal of the limit cycle in the λ_a dependence of $V(p, p, \lambda_a)$ for $p \sim \sigma$. In this region, the evolution of the alternative generators is distinctively different from the standard T generator but not heavily suppressed as for large $p \gg \sigma$. In practice, many oscillatory features are compressed in the region $p \sim \sigma$ and thus can be distinguished from other effects of the evolution. They can be used to extract the preferred scaling factor numerically.

5 Summary and Outlook

In this paper, we have investigated the renormalization group limit cycle of the quantum-mechanical $1/R^2$ potential within the similarity renormalization group framework. We showed that the period of the limit cycle can be extracted from the λ_a dependence of the diagonal elements of the evolved interaction $V(p, p, \lambda_a)$ if the alternative generators in Eq. (8) with a dimensionful parameter σ are used. In the region $p \sim \sigma$ sufficiently many oscillatory features are present, such that a numerical extraction of the preferred scaling factor is possible. Here, we have determined the period simply by taking averages over the positions of minima and maxima in $V(p, p, \lambda_a)$. More elaborate statistical analysis schemes using Bayesian statistics can help to improve the extraction of the period [22].

In the future, it will be interesting to apply our technique to the nuclear three-body system in order to derive the limit cycle in the pionless EFT from a more fundamental chiral interaction with explicit pions. Work in this direction is in progress.

Acknowledgements. Useful discussions with Dick Furnstahl and Lucas Platter are gratefully acknowledged. This work was supported in part by the Helmholtz Association under contract HA216/EMMI, by the BMBF (grant 06BN9006), and by the DFG through SFB 634.

References

1. E. Braaten, and H.-W. Hammer, "Universality in Few-body Systems with Large Scattering Length," Phys. Rept. **428**, 259 (2006) [arXiv:cond-mat/0410417].
2. V. Efimov, "Energy Levels Arising from Resonant Two-body Forces in a Three-body System," Phys. Lett. **33B**, 563 (1970).
3. S. Albeverio, R. Hoegh-Krohn, and T.S. Wu, "A Class of Exactly Solvable Three-body Quantum Mechanical Problems and the Universal Low-energy Behavior," Phys. Lett. **83A**, 105 (1981).
4. P. F. Bedaque, H.-W. Hammer, and U. van Kolck, "Renormalization of the three-body system with short-range interactions," Phys. Rev. Lett. **82**, 463 (1999) [arXiv:nucl-th/9809025]; "The Three-Boson System with Short-Range Interactions," Nucl. Phys. A **646**, 444 (1999) [arXiv:nucl-th/9811046].
5. R. F. Mohr, R. J. Furnstahl, R. J. Perry, K. G. Wilson and H.-W. Hammer, "Precise numerical results for limit cycles in the quantum three-body problem," Annals Phys. **321**, 225 (2006) [nucl-th/0509076].
6. F. Ferlaino, and R. Grimm, "Forty years of Efimov physics: How a bizarre prediction turned into a hot topic," Physics **3**, 9 (2010).
7. C. Chin, R. Grimm, P. Julienne, and E. Tiesinga, "Feshbach Resonances in Ultracold Gases," Rev. Mod. Phys. **82**, 1225 (2010) [arXiv:0812.1496].
8. A. Zenesini, B. Huang, M. Berninger, S. Besler, H.-C. Nägerl, F. Ferlaino, R. Grimm, C. H. Greene, and J. von Stecher, "Resonant Five-Body Recombination in an Ultracold Gas," New J. Phys. **15**, 043040 (2013) [arXiv:1205.1921].
9. S.-K. Tung, K. Jimenez-García, J. Johansen, C. V. Parker, and C. Chin, "Geometric Scaling of Efimov States in a 6-Li–133-Cs Mixture," Phys. Rev. Lett. **113**, 240402 (2014) [arXiv:1402.5943].
10. R. Pires, J. Ulmanis, S. Häfner, M. Repp, A. Arias, E.D. Kuhnle, and M. Weidemüller, "Observation of Efimov Resonances in a Mixture with Extreme Mass Imbalance," Phys. Rev. Lett. **112**, 250404 (2014) [arXiv:1403.7246].
11. H. -W. Hammer and L. Platter, "Efimov States in Nuclear and Particle Physics," Ann. Rev. Nucl. Part. Sci. **60**, 207 (2010) [arXiv:1001.1981 [nucl-th]].

12. F. Wegner, "Flow Equations for Hamiltonians," Ann. Phys. (Leipzig) **3**, 77 (1994).
13. S. D. Glazek and K. G. Wilson, "Renormalization of Hamiltonians," Phys. Rev. D **48**, 5863 (1993); "Perturbative renormalization group for Hamiltonians," Phys. Rev. D **49**, 4214 (1994).
14. S. K. Bogner, R. J. Furnstahl and A. Schwenk, "From low-momentum interactions to nuclear structure," Prog. Part. Nucl. Phys. **65**, 94 (2010) [arXiv:0912.3688 [nucl-th]].
15. R. J. Furnstahl and K. Hebeler, "New applications of renormalization group methods in nuclear physics," Rept. Prog. Phys. **76**, 126301 (2013) [arXiv:1305.3800 [nucl-th]].
16. E. D. Jurgenson, P. Maris, R. J. Furnstahl, P. Navratil, W. E. Ormand and J. P. Vary, "P-shell nuclei using Similarity Renormalization Group evolved three-nucleon interactions," Phys. Rev. C **87**, 054312 (2013) [arXiv:1302.5473 [nucl-th]].
17. K. Hebeler and R. J. Furnstahl, "Neutron matter based on consistently evolved chiral three-nucleon interactions," Phys. Rev. C **87**, 031302 (2013) [arXiv:1301.7467 [nucl-th]].
18. S. Kehrein, *The flow equation approach to many-particle systems*, Springer, Berlin/Heidelberg (2006).
19. W. Li, E. R. Anderson and R. J. Furnstahl, "The Similarity Renormalization Group with Novel Generators," Phys. Rev. C **84**, 054002 (2011) [arXiv:1106.2835 [nucl-th]].
20. H. -W. Hammer and B. G. Swingle, "On the limit cycle for the $1/r^2$ potential in momentum space," Annals Phys. **321**, 306 (2006) [quant-ph/0503074].
21. S. D. Glazek, "Limit cycles of effective theories," Phys. Rev. D **75**, 025005 (2007) [hep-th/0611015].
22. R. J. Furnstahl, D. R. Phillips and S. Wesolowski, "A recipe for EFT uncertainty quantification in nuclear physics," J. Phys. G **42**, 034028 (2015) [arXiv:1407.0657 [nucl-th]].